Stimulated rotational Raman generation controlled by strongly driven vibrational coherence in molecular deuterium

A. M. Burzo,[*] A. V. Chugreev,[†] and A. V. Sokolov

Department of Physics and Institute for Quantum Studies, Texas A&M University, College Station, Texas 77843-4242, USA
(Received 30 October 2006; published 26 February 2007)

We report an experimental observation of simultaneous rotational and vibrational collinear Raman generation in low pressure cooled deuterium gas, with only two narrow-band laser pulses applied at the input of the molecular cell. Only the fundamental vibrational transition Q_1 (0) is driven strongly in this experiment. However, in addition to efficient vibrational Raman generation we observe generation of a large number of rotational sidebands (more than 100) corresponding to S_0 (0) transition. We notice that fine-tuning of the frequency difference of the driving fields near the vibrational Raman resonance changes dramatically the aspects of the generated spectrum and the efficiency of rotational generation: from complete suppression of a self-starting stimulated rotational Raman generation to a strong enhancement of two orders of magnitude. We conduct a numerical analysis that allows us to attribute this behavior to quantum interference among the probability amplitudes of the three molecular states involved.

I. INTRODUCTION

Production of subfemtosecond optical pulses requires a broadband source of coherent radiation, and has been recently accomplished by high harmonic generation [1,2]. The time scale of such pulses makes them suitable for probing the motion of innershell electrons, which are tightly bound to the nuclei, or could provide information about fast ionization processes [3]. Molecular modulation is an alternative technique which results in production of a discrete spectrum of sidebands spaced by the frequency of the driven molecular oscillation [4–6] and synthesize pulses of single cycle duration [7,8]. Molecular modulation (or collinear Raman generation) relies on adiabatic preparation of a coherent molecular ensemble by two laser fields tuned close to a Raman resonance, which results in production of a discrete spectrum of sidebands spaced by the molecular frequency. Related work includes proposed [9,10] and demonstrated [11] ultrashort pulse compression by impulsive Raman scattering, as well as proposed production of adiabatic [12] and nonadiabatic [13] solitons. Providing an important improvement to the molecular modulation technique, Harris and co-workers have recently investigated the possibility of producing a denser comb of frequencies (which synthesizes a train of pulses with longer average pulse delay and higher peak intensity, and allows more flexibility for pulse shaping) by simultaneous rotational and vibrational collinear Raman generation [14,15]. They used three lasers to drive two Raman transitions in two different molecular species. A similar idea of using three lasers in order to drive two Raman transitions in the same gas was also demonstrated [16].

We find that collinear rotational and vibrational generation can occur simultaneously in the same molecular gas with only two laser fields applied and only one (vibrational)

transition driven strongly. Moreover, we determine that vibrational excitation can be used to control rotational Raman generation.

The paper is organized as follows. Section II provides a brief overview of related work in stimulated Raman scattering. Sections III and IV describe our experimental setup, the conditions of our observation, and the results of our experiments. We obtain broadband collinear vibrational Raman generation (molecular modulation) within a reasonably wide range of Raman detunings from the vibrational resonance. At the same time we observe (self-starting) stimulated rotational Raman generation that is present even when one laser pulse is applied, but is strongly affected by vibrational Raman generation when both lasers are applied. Section V shows that fine-detuning of the driving fields near the vibrational Raman resonance has a dramatic influence on the rotational Raman generation: from a complete suppression to a strong enhancement. In Sec. VI we provide a theoretical analysis that allows us to attribute this behavior to quantum interference among the probability amplitudes of the three molecular states involved.

II. PREVIOUS WORK

Stimulated Raman scattering (SRS) has been studied extensively, in light of its applications to frequency conversion and multiple wavelength generation. Raman process can be described by inelastic scattering of a laser beam in a medium, which results in either up converted frequencies (anti-Stokes lines) or down converted frequencies (Stokes lines) shifted by a rotational or vibrational energy in a molecule. If the intensity of the laser beam is sufficiently high, then stimulated scattering becomes substantial, and leads to an exponential growth of the total scattered light [17].

Different media (gases, solids, or liquids) subjected to pump pulses of different duration, have been employed to investigate this effect [18–21]. Of particular pertinence is the generation of rotational SRS arising from S_0 (0) transition in deuterium at liquid nitrogen temperatures by the second har-

---

*Electronic address: andrea@physics.tamu.edu
†Current address: Department of Physics, Umeå University, Sweden.

monic (532 nm) of a nanosecond Nd:YAG laser [22]. How-
ever, the pressure used in that experiment was high (8 atm,
consistent with normal conditions at which stimulated Ra-
man scattering occurs).

Other work reported the use of a single dye laser operat-
ing at two different wavelengths separated by roughly the
energy difference between two rotational levels in hydrogen
[23] for generation of around 40 lines through a two-color-
induced stimulated Raman effect. By introducing the two-
color laser beam, the threshold of rotational generation was
greatly reduced. In further work, the same team maximized
the number of generated lines by tuning this time the fre-
quencies of two lasers to exactly match their frequency dif-
ference to a rotational transition frequency in hydrogen [24].
The Stokes and anti-Stokes lines were generated by the com-
bined effects of stimulated Raman scattering and four wave
mixing (FWM) in a phenomenon called "Stokes" cascading.
Since the two-color-induced Raman spectra consisted of
equidistant lines, a mechanism of generating ultrashort laser
pulses was suggested later [25]. As a first step towards
achieving this goal, Imasaka's group [26] generated a pure
rotational comb of frequencies, effectively suppressing vi-
brational generation by optimizing gas pressure, focusing
conditions, and polarization of their two lasers. Enhance-
ment of rotational SRS was shown by operating at low pressure of
Raman medium, while larger pressures favored vibrational
generation. In addition, the use of circularly polarized pump
beams favored the efficient rotational stimulated Raman scat-
tering.

As it was shown before, focusing geometry influences
greatly the SRS process. Tight focusing conditions result in a
gain suppression due to stronger Stokes and anti-Stokes cou-
pling [27]. The gain suppression in the case of nonresonant
SRS occurred when the angles of exact phase matching con-
dition for Stokes and anti-Stokes were maintained within
confocal volume of the pump beam [28]. Furthermore, the
same group [28] demonstrated experimentally that it is pos-
sible to enhance either pure rotational or pure vibrational
SRS in hydrogen at the same pump energy and pressure of
the Raman gas. The enhancement of one transition or another
was realized by proper focusing conditions which lead to
parametric gain suppression of the rival process. However, to
our knowledge, no work has been reported that shows the
enhancement or suppression of rotational Raman generation
depending on the vibrational Raman detuning, at exactly the
same conditions of pressure, intensities of driving fields, and
focusing geometry.

III. EXPERIMENTAL SETUP

The experimental setup is similar to the one in Ref. [6]
and is presented in Fig. 1. Two lasers with a frequency dif-
ference tunable around vibrational frequency corresponding
to the $Q_1 (0)$ transition in deuterium are send into a liquid
nitrogen cooled cell (T=77 K). The pressure of deuterium
varied from 50 to 750 Torr in different experiments. In Fig.
2 we present a few of the vibrational and rotational energy
levels in deuterium together with their corresponding transi-
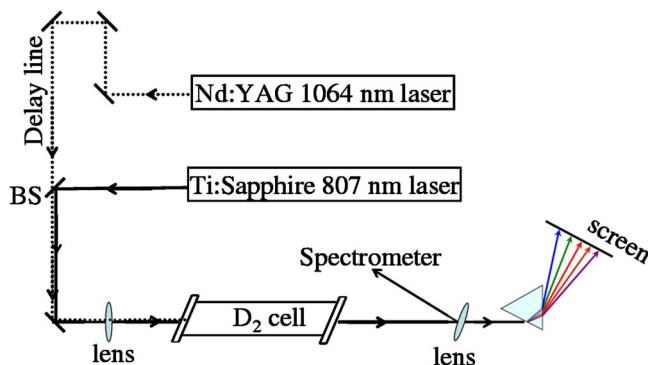tion frequencies.

FIG. 1. (Color online) Experimental setup for collinear Raman
generation in deuterium. Fundamental vibrational transition [$Q_1 (0)$]
is driven by two transform-limited laser pulses with wavelengths of
1064 and 807 nm. Their tunable frequency difference is approxi-
mately equal to the vibrational frequency of 2994.6 cm^{-1}.

The first laser is a Q-switched injection seeded Nd:YAG
laser (Quanta-Ray 6350) with pulse duration t_p=12 ns at the
fundamental 1064 nm wavelength. These pulses are near
transform limited, and the corresponding linewidth is given
by $\delta\omega_{1064\ nm} \approx \frac{2 \ln(2)}{\pi t_p} \approx 37$ MHz. The output energy of the
1064 nm laser was attenuated by a pinhole to a maximum
value of 240 mJ/ pulse, at a repetition rate of 10 Hz. We use
the second harmonic of this fundamental pump frequency to
pump the second laser used in our experiment, which is an
injection seeded tunable home-build Ti:sapphire laser oper-
ating at the 807 nm wavelength. The construction of this
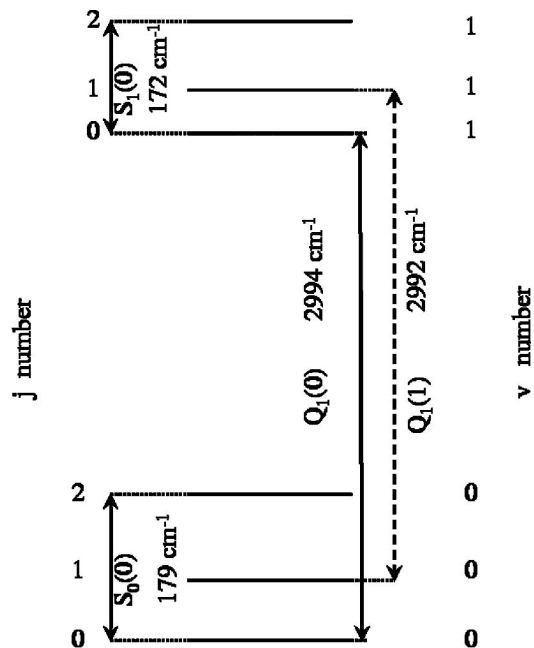cavity is different than the one used in previous experiments

FIG. 2. Energy diagram of different Raman transitions in deu-
terium. The only transition driven in our experiment is $Q_1 (0)$. In
addition to strong collinear generation of multiple $Q_1 (0)$ Raman
sidebands, we experimentally observe numerous multiple-order
Stokes and anti-Stokes sidebands corresponding to the $S_0 (0)$
transition.

[5]. Specifically, the cavity round-trip length was reduced to approximately 10 cm in order to achieve shorter time duration of the output pulses. Since the coherence lifetime of a dipole-forbidden transition is limited by the collisional dephasing rate (which is proportional to the gas pressure), shorter pulses allow us to work with large ensemble densities, which results in an increase of the efficiency of the generation process. The output energy of the injection seeded Ti:sapphire laser reaches 18 mJ/pulse with a pulse duration of about 5 ns and a linewidth $\delta\omega_{Ti:sapph}$ of about 90 MHz. The temporal synchronization of the two driving fields is achieved by building a delay line for the 1064 nm laser.

Polarizations of the two driving fields are linear, with ellipticities of 0.08 for the 807 nm laser and 0.03 for the 1064 nm laser. Explicit details of the polarization measurement procedure can be found in Ref. [29]. The wavelength monitoring was done with a Burleigh WA 1500 wavemeter (resolution of 40 MHz).

The two pulses are combined on a dichroic beamsplitter and focused by a 75 cm lens to spot sizes of 275 μm (807 nm laser) and 265 μm (1064 nm laser). Two extra pairs of lenses were used for both beams for better adjustment of focusing points and beam sizes, which resulted in a divergence of the Ti:sapphire laser of 7.3 mrad, and 2.7 mrad for Nd:YAG 1064 nm laser.

The two lasers are focused in the middle of a 1.2 m long liquid nitrogen cooled cell with fused silica windows cut at Brewster angle. By cooling the cell to $T=77$ K, we increase the population in the $J=0$ state to 66%, and reduce the Doppler linewidth of the transition.

A bright white beam of light is observed at the output of the cell when the frequency difference of the two lasers is tuned to within few GHz from the vibrational Raman resonance. Dispersing the white output light by a pair of fused silica prisms allowed us to resolve a fine structure [later identified as corresponding to the lowest rotational transition S_0 (0)], which appeared around each one of the main vibrational lines. This spectrum is recorded by an Ocean Optics spectrometer (HR4000-UV-VIS-NIR) equipped with 3648-element CCD-array detector with a detection range from 200 to 1100 nm (see Fig. 3). The measurement procedure is as follows: at the output of the cell, a 1000 mm antireflection coated lens is used to focus the spectrum dispersed by the prisms and project it onto a white screen placed at 3 m away from the exit window of the cell. The lens is slightly tilted in order to send a small reflection backwards to an aluminum foil, which then scatters the reflected light into the fiber spectrometer. Due to the collection geometry, the 1064 nm beam is attenuated relative to other beams.

The origin of the rotational generation is stimulated Raman scattering of the 1064 nm Nd:YAG laser, a process that occurs (as we have concluded) in the transient time regime, since the lifetime of optical phonons for S_0 (0) transition in our working pressure range from 50 to 750 Torr and at a temperature of 77 K [30] is comparable to our Nd:YAG pulse duration of 12 ns. We observe the onset of SRS with Nd:YAG laser only at pressures above 250 Torr, and energies above 180 mJ/pulse. Increasing the 1064 nm pump power results in a linear increase of the efficiency of rotational generation, and in generation of a Stokes and anti-
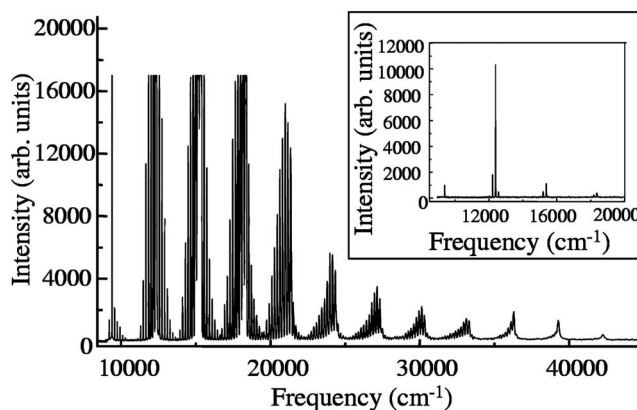

FIG. 3. A typical spectrum obtained in molecular deuterium as recorded by a spectrometer (Ocean Optics HR4000CG-UV-NIR). This spectrum is produced by a combination of collinear Raman generation as described in Ref. [6] [with efficient excitation of the Q_1 (0) vibrational transition] and SRS at the S_0 (0) rotational transition. Detuning from the vibrational Raman resonance is $\Delta\omega$ =1.61 GHz. The 807 nm laser energy is 8 mJ/pulse, while the energy of the 1064 nm laser is 240 mJ/pulse, and D_2 pressure is 300 Torr. The inset shows the unsaturated spectrum obtained by reducing the intensity by a factor of 100.

Stokes cascading process. These results are shown in Fig. 4. Here the intensities of the generated Stokes (circles) and anti-Stokes (triangles) are measured by the spectrometer, with the background noise subtracted from the plot. Due to the limited range of our spectrometer, higher-order Stokes sidebands are not detected, but an anti-Stokes SRS cascading spectrum can be seen in Fig. 4 (inset) at a pressure of
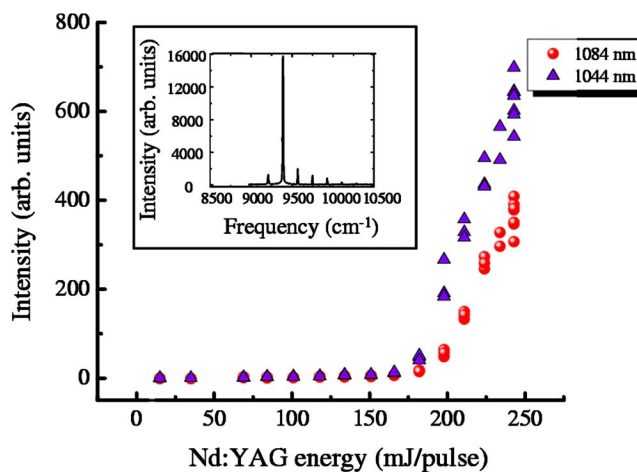

FIG. 4. (Color online) The first Stokes (1084 nm, circles) and anti-Stokes (1044 nm, triangle) intensities as function of the input pulse energy, when only the Nd:YAG (1064 nm) laser is applied at the input of the deuterium cell. These intensities were measured at the exit of the cell by sending a small portion of the output beam into the spectrometer. The background noise was subtracted from the data. The inset shows the cascading anti-Stokes process observed when the Nd:YAG pump energy is at 240 mJ/pulse. Stokes cascading behavior is not visible here due to the limited detection spectral range. The pressure in the Raman cell was 300 Torr and the temperature was 77 K.

300 Torr and a pump pulse energy of 240 mJ/pulse.

One would expect that increasing the pressure in the cell results in a more efficient rotational generation. However, additional side effects (backward SRS or gas breakdown) are observed that tend to reduce the rotational Raman gain. In order to avoid them, the deuterium pressure needs to be optimized. For example, at a pressure of 749 Torr, we have observed that in addition to the rotational Stokes at 1084 nm, a stimulated vibrational sideband appears at a wavelength of 830 nm. Another problem that arises at high pressures and high intensities of the driving fields is gas breakdown due to efficient UV generation produced in high-order vibrational anti-Stokes processes. Above 100 Torr and for pump pulses durations of few nanoseconds, gas breakdown occurs due to an electron avalanche generated by repeated inverse bremsstrahlung absorption [31] with the seed ions produced by the multiphoton ionization (which is greatly enhanced when UV light is present). The effect of laser induced breakdown was studied for example in deuterium with 4 ns pump pulses in the pressure range of 800 Torr [32]. From the dependence of threshold breakdown intensity on pressure it was inferred that breakdown occurs due to the growth of inverse bremsstrahlung absorption which is unaffected by recombination or diffusion processes.

Therefore, in order to avoid ionization and other parasitic processes, we chose to conduct further experiments at a lower pressure (below 300 Torr) and at lower pump pulse energies [8 mJ/pulse (807 nm laser), and 150 mJ/pulse (1064 nm laser)] corresponding to the threshold of the forward rotational SRS process.

IV. DETERMINATION OF PRECISE RAMAN RESONANCE

We have observed that at a fixed pressure and given energies of driving fields, rotational generation completely disappears as the detuning from the vibrational Raman resonance is changed, while at a different detuning the rotational generation is enhanced. As a first step, we determine the position of the vibrational Raman resonance by tuning the Ti:sapphire laser frequency and measuring the first anti-Stokes sideband generation at the 650 nm wavelength. This measurement (shown in Fig. 5) is done at a pressure of 289 Torr and with driving fields attenuated such that only this first anti-Stokes sideband is generated. Here detunings are shown by keeping the convention from Ref. [4] (negative detuning is indicated in the inset in Fig. 5). The position of the Raman resonance at our working pressure of 300 Torr was confirmed by repeating the previous measurement at two other pressures and extracting the linear shift of the Raman resonance with pressure.

All spectra were taken while monitoring and recording the power transmitted through the cell and the acoustic signal from a microphone placed inside the cell and connected to an oscilloscope. These two measurements illustrate the evolution of the molecular system (adiabatic or nonadiabatic), as described also in Ref. [5]. If the ensemble of molecules is prepared adiabatically into a single eigenstate which initially coincides with the ground state, then we expect that after
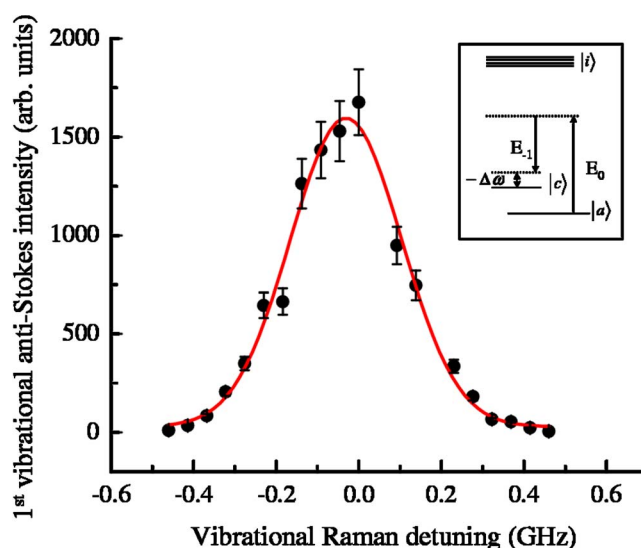

FIG. 5. (Color online) Generated intensity of the first vibrational anti-Stokes sideband (at 650 nm) as a function of the vibrational Raman detuning in deuterium at a pressure of 289 Torr and a temperature of 77 K. Energies of driving fields were 1 mJ/pulse for the 1064 nm beam, and 8 mJ/pulse for the 807 nm laser. The exact wavelength of the 807 nm laser, which corresponds to the vibrational Raman resonance (zero detuning) was determined to be 807.2122 from the measured intensities (as indicated by the wave meter). The solid line shows the Gaussian fit to the data. Error bars roughly correspond to 10% of the intensity fluctuations. As shown in the inset, the two-photon detuning from the vibrational Raman resonance $\Delta\omega$ is negative when the laser frequency difference is larger than the molecular frequency.

pulses are gone, all molecules will return to the ground state, meaning no energy is left in the system. Close to the Raman resonance, the adiabaticity condition is not satisfied, and some of the driving field energy is absorbed by the molecules, exciting the molecular states. The molecular excitation is followed quickly by a relaxation process, and by the excitation energy dissipating into heat and producing a strong shock wave, which is picked up by the microphone.

These two measurements are shown in Fig. 6. We observe that the dip in the transmitted energy is shifted substantially from the Raman resonance due to higher intensities of the applied fields than previously employed, which results in larger Stark shifts [5,33]. A simple estimate of the magnitude of this shift, taking into account only the presence of the driving fields (at their peak intensity), yields a value of -1.1 GHz. The relatively large two photon Rabi frequency for our experimental conditions (about 0.6 GHz) compared to the typical values of few tens of MHz employed in previous experiments [5,33] results in a somewhat larger energy loss in the system (about 15%).

V. ENHANCEMENT AND SUPPRESSION OF ROTATIONAL GENERATION AS A FUNCTION OF VIBRATIONAL RAMAN DETUNING

We have observed the influence of the vibrational Raman generation on the efficiency of the rotational Raman genera-
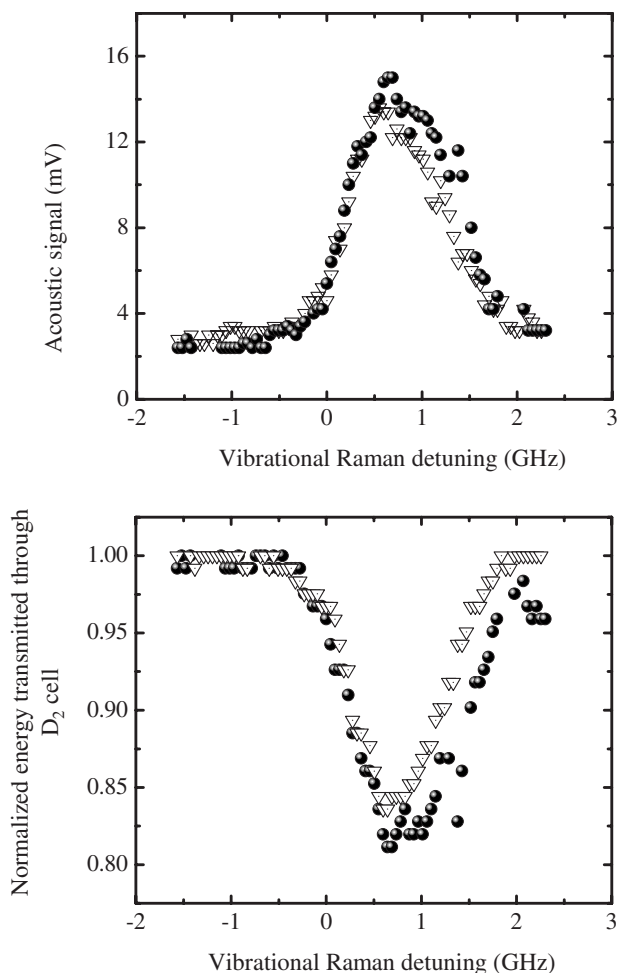
FIG. 6. Acoustic signal as measured by a microphone placed inside the cell (top figure) and normalized power transmitted through the cell as measured by a power meter (bottom figure) as a function of the vibrational Raman detuning. The data was normalized to the power transmitted at large detunings. Circles correspond to a first scan, while triangles indicate a second scan taken at a later time.

tion. This effect is very intriguing and the explanation of the observed behavior is not obvious. We have studied in detail the experimental conditions of the enhancement or suppression of the rotational generation, and further suggest a theoretical model that provides a qualitative analysis of this effect. Figures 7 and 8 show two extreme situations: efficient vibrational generation with complete suppression of the rotational generation (Fig. 7) and efficient vibrational-rotational generation (Fig. 8). The only difference between the two cases is the detuning from the vibrational Raman resonance (exact resonance in the first case, and 1.15 GHz positive detuning in the second case).

The intensities of the rotational Stokes and anti-Stokes lines in the vicinity of 1064 nm laser line were monitored together with intensities of all other rotational and vibrational lines as the detuning from the vibrational Raman resonance was changed. These dependencies are shown in Fig. 9 for rotational [parts (a) and (b)] and vibrational [part (c)] sidebands. We denote the intensities of the rotational Stokes
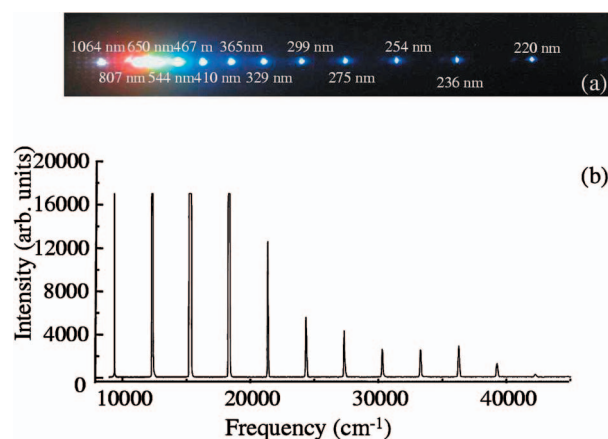

FIG. 7. (Color) The spectrum generated in D_2, consisting only of vibrational lines. The 807 nm laser energy is 8 mJ/pulse, while the energy of the 1064 nm laser is 180 mJ/pulse, and the D_2 pressure is 300 Torr. The detuning from the vibrational Raman resonance is 0 GHz. Part (a) represents a picture of the dispersed spectrum taken with a digital camera, while (b) shows the same spectrum as recorded by the spectrometer (Ocean Optics HR4000CG-UV-NIR) (adapted from Ref. [29]).

1084 nm sideband by triangles, the anti-Stokes 1044 nm sideband by circles, the Ti:sapphire anti-Stokes sideband (at 795 nm) by diamonds, and the Ti:sapphire Stokes sideband (at 818 nm) by stars. The intensity of the 818 nm sideband at positive detunings saturated the detector. Part (c) shows the behavior of the vibrational sideband at 650 nm (filled circles), and at 532 nm (crosses) as the detuning from the Raman resonance is changed. These intensities were attenuated by a factor of 100 (compared to rotational sidebands). A very similar behavior is observed for all other vibrational sidebands. Each data point on the curve represents an average over 30 shots.

The behavior of vibrational lines as a function of detuning is as expected, and is similar to the one observed, for ex-
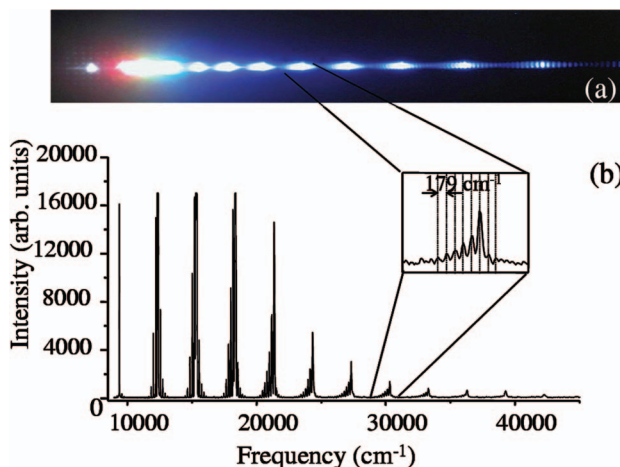

FIG. 8. (Color) Vibrational-rotational comb of sidebands obtained at 300 Torr pressure and 1.15 GHz detuning. Part (a) represents a picture of the dispersed spectrum, while (b) illustrates the same spectrum as recorded by the spectrometer. The inset shows the rotational comb spaced by 179 cm^{-1} (figure adapted from Ref. [29]).
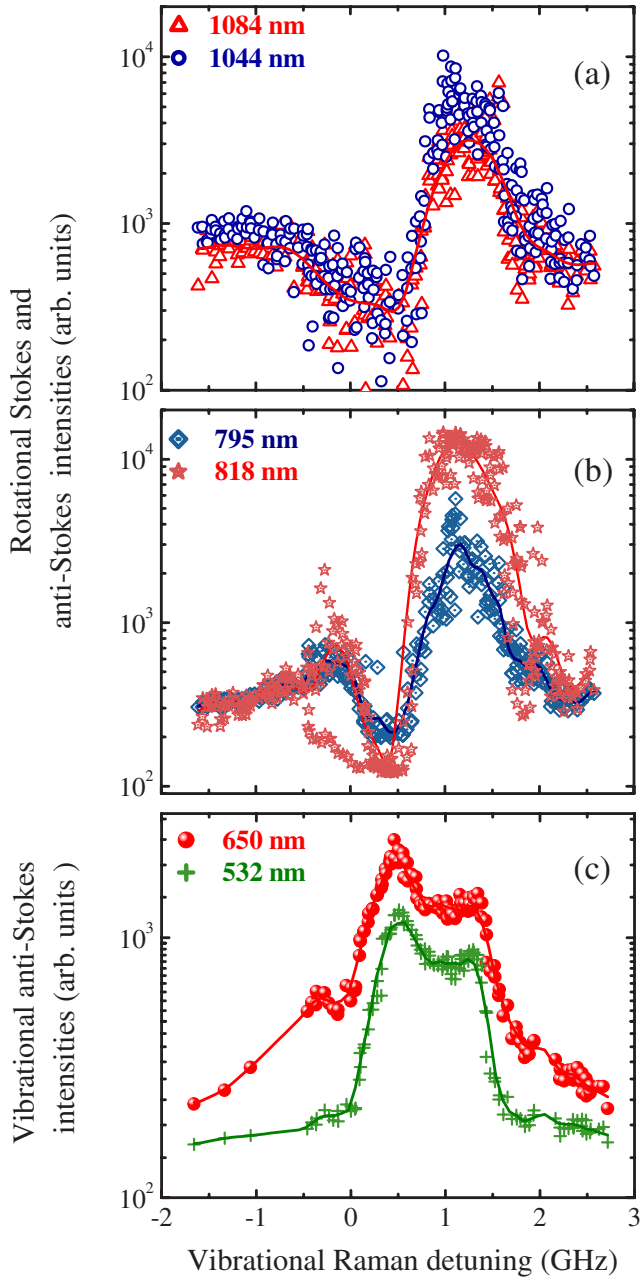
FIG. 9. (Color online) Intensities of the rotational Stokes and anti-Stokes sidebands (a) and (b) and the vibrational anti-Stokes sidebands (c) produced by the two input lasers (1064 and 807 nm) as a function of their detuning from the vibrational Raman resonance. In part (a) triangles show rotational Stokes at 1084 nm and circles show rotational anti-Stokes at 1044 nm. In part (b) stars show rotational Stokes at 818 nm, while diamonds indicate rotational anti-Stokes at 795 nm. The intensity of 818 nm sideband is saturated at positive detunings. The vibrational anti-Stokes intensities are shown in part (c) attenuated by a factor of 100. Filled circles indicate vibrational sideband at 650 nm and crosses indicate second anti-Stokes sideband at 532 nm. The solid curves represent five point smoothing of the data and are meant to guide the eye. Each data point corresponds to an integration time of 3 s, and therefore represents the average of 30 output spectra. The intensities are measured with a spectrometer (Ocean Optics HR4000CG-UV-NIR).
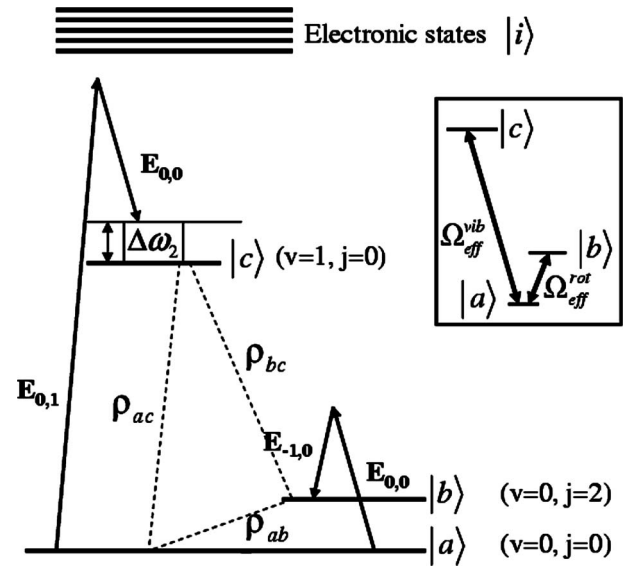

FIG. 10. Schematics of the proposed quantum interference mechanism. Two Raman transitions are driven by three laser fields in an effective Raman V scheme (inset). Rotational transition S_0 (0) is driven by the 1084 nm ($E_{-1,0}$) rotational Stokes sideband and the Nd:YAG ($E_{0,0}$) 1064 nm laser. Vibrational transition Q_0 (1) is driven by the 807 nm ($E_{0,1}$) laser and the Nd:YAG ($E_{0,0}$) at 1064 nm. The transition ($v''=0, j''=2 \rightarrow v'=1, j'=0$) is Raman allowed. The rotational-vibrational comb is generated as a result of an interference of contributions produced by coherences ρ_{ab}, ρ_{ac}, ρ_{bc}, with appropriate phasing for different Raman detunings from the vibrational resonance.

ample, in Ref. [5]. For negative detunings vibrational generation is less efficient than for positive detunings. On-resonance generation, is overall less efficient than off-resonance one [5].

Rotational lines show similarly complex behavior. Close to the vibrational Raman resonance, suppression of the rotational Stokes and anti-Stokes sidebands around the 1064 nm line indicates that the two Raman processes are interconnected.

We also notice that the efficient generation occurs with the nonadiabatic evolution of the system. This result is in agreement with recent experimental observations [33]. The authors point out that increasing the two-photon Rabi frequency of the driving fields results in a more efficient generation, although the non-adiabatic behavior of the system becomes more pronounced. In addition, larger two-photon Rabi frequency makes the generation efficiency dependence on detuning less pronounced [33], and explains the efficient generation that occurs at vibrational Raman detunings as large as few GHz (Fig. 9).

VI. THEORETICAL EXPLANATIONS AND CONCLUSIONS

An intriguing hypothesis that we first considered for the explanation of the enhanced rotational generation, was the temporal compression (by the normal dispersion of the molecular medium itself) of the ultrashort pulses synthesized by the vibrational Raman sidebands. Even though such com-

pression is expected to occur for the antiphased state (at negative Raman detunings), it has been pointed out that it can also occur at positive detunings in a nonadiabatic regime [34]. Ultrashort pulse compression (due to the vibrational Raman generation) could potentially enhance the rotational generation, but it appears that a more plausible scenario exists, as shown further below.

Another phenomenon that could affect the rotational sideband intensities is Raman self-focusing [35]. This kind of self-focusing occurs when two lasers drive a Raman transition with the laser frequency difference slightly detuned from the Raman resonance. The changes in refractive index result in changes of beam propagation, and therefore occurrence of self-focusing or defocusing, depending on the sign of the detuning. Experimental results using the rotational transition S_1 (0) in hydrogen [35] have demonstrated that self-focusing occurs at 0.6 GHz from Raman resonance, with a beam size changing by as much as 40% as detuning is changed from antiphased to phased state. This self-focusing could increase the gain of SRS, resulting then in a more efficient rotational generation. As shown in the same experimental work [35], defocusing occurs at very small negative detunings from the Raman resonance, and may contribute to the suppression of rotational lines. However, no substantial self-focusing or defocusing was observed under our experimental conditions.

Our analysis suggests that the interplay of vibrational-rotational generation could be a result of quantum interference (EIT-like) among the probability amplitudes of the three molecular states involved. To verify this hypothesis, we consider that in addition to the vibrational coherence between the ground vibrational state and the first excited vibrational state ($v''=0, j''=0 \rightarrow v'=1, j'=0$), a rotational coherence is established between the ground vibrational state and the second ground rotational state ($v''=0, j''=0 \rightarrow v'=0, j'=2$). We

assume that this rotational transition is driven by the first rotational Stokes sideband at 1084 nm (which appears due to the SRS) and the Nd:YAG 1064 nm. This suggested schematic is shown in Fig. 10.

Due to the Raman selection rules, the transition ($v''=0$, $j''=2 \rightarrow v'=1, j'=0$) is allowed, and a coherence between the states $|b\rangle$ and $|c\rangle$ is induced by the applied fields. As more sidebands are generated later in the cell, the "induced coherence" creates additional fields driving these two states. Our goal is to calculate the intensities of the generated sidebands (rotational and vibrational) at particular detunings from the vibrational Raman resonance and to compare them with our experimental results.

Therefore, we start by assuming that the electric field of the applied and the generated sidebands is described in terms of the complex envelope quantity $\hat{E}_{q,p}(z.t)$:

$$\hat{E}_{q,p}(z,t) = Re\{E_{q,p}(z,t)\exp[j(\omega_{q,p}t - k_{q,p}z)]\}, \quad (1)$$

where $\omega_{q,p}=q\omega_{m1}+p\omega_{m2}$ and $k_{q,p}=\frac{\omega_{q,p}}{c}$. The index q is an integer which labels rotational sidebands, and the index p corresponds to vibrational sidebands. We indicate by ω_{m1} the modulation frequency (179 cm^{-1}) of the rotational transition, i.e., the frequency difference between rotational driving field frequencies $E_{-1,0}$ and $E_{0,0}$. Similarly, ω_{m2} represents the vibrational modulation frequency which is set by the difference of vibrational driving frequencies $E_{0,1}$ and $E_{0,0}$ (roughly 2994 cm^{-1}).

Following the approach of Ref. [4], we assume that the detunings of the laser fields from electronic states are large compared to Rabi frequencies, and that the probability amplitudes of these states are small. Therefore, this system can be described by an effective 3×3 Hamiltonian, given by

$$H = -\frac{1}{2} \begin{pmatrix} \sum_{q,p} a_{q,p}|E_{q,p}|^2 & \sum_{q,p} b_{q,p}^1 E_{q,p}E_{q-1,p}^* & \sum_{q,p} b_{q,p}^2 E_{q,p}E_{q,p-1}^* \\ \sum_{q,p} b_{q,p+1}^{1*} E_{q,p}E_{q+1,p}^* & 2\Delta_1 - \sum_{q,p} d_{q,p}^1|E_{q,p}|^2 & \sum_{q,p} b_{q,p}^3 E_{q,p}E_{q+1,p-1}^* \\ \sum_{q,p} b_{q,p+1}^{2*} E_{q,p}E_{q,p+1}^* & \sum_{q,p} b_{q-1,p+1}^{3*} E_{q,p}E_{q-1,p+1}^* & 2\Delta_2 - \sum_{q,p} d_{q,p}^2|E_{q,p}|^2 \end{pmatrix}. \quad (2)$$

Here the result is derived assuming that the two photon detunings are Δ_1 from rotational Raman resonance (which for our case is zero), and Δ_2 from the vibrational Raman resonance. The terms $a_{q,p}$, $b_{q,p}^1$, $b_{q,p}^2$, $b_{q,p}^3$, $d_{q,p}^1$, and $d_{q,p}^2$ represent the dispersion and the coupling coefficients for rotational, vibrational, and rovibrational transitions. Their expressions are given in the Appendix.

We assume that the two transitions are driven by fields with a Gaussian temporal profile, and with pulse durations and intensities similar to our experimental conditions: 12 ns and 5 GW/cm^2 peak intensity for the Nd:YAG laser, and

5 ns and 0.8 GW/cm^2 for the Ti:sapphire laser. The rotational sideband at 1084 nm is assumed to have a pulse duration equal to the one corresponding to the Nd:YAG laser and an intensity equal to 1% of the peak intensity of the Nd:YAG laser.

Next, we solve the time dependent Schrödinger equation with initial condition corresponding to the case when all population is in the ground state, and we calculate the time dependent values of the populations and coherences as a function of the vibrational Raman detuning. We make sure to keep track of the relative signs of the Franck-Condon factors
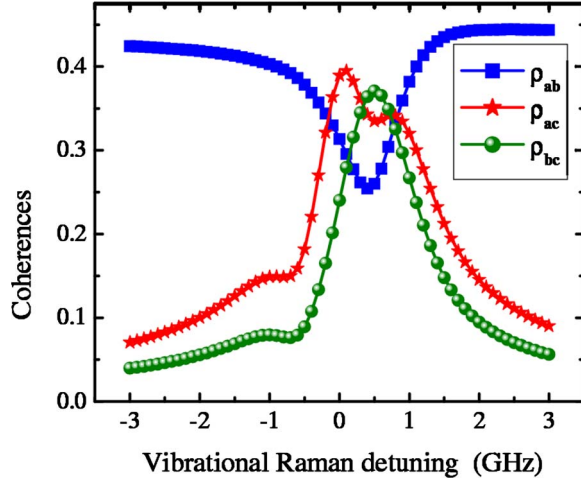
FIG. 11. (Color online) Calculated rotational (blue squares), vibrational (red stars), and ro-vibrational (green circles) coherences at a time $t=0$ which corresponds to the applied peak intensity as a function of the vibrational Raman detuning. The only fields assumed to be present are 1064, 1084, and 807 nm, with Gaussian temporal profiles, and durations and intensities comparable with our experimental conditions. The results are obtained by solving the time dependent Schrödinger equation, assuming that all population is initially in the ground state.

when solving the time dependent Schrödinger equation, since these factors dictate the relative sign of the coherences. The results of this calculation at a time $t=0$ corresponding to the peak of the pulses are shown in Fig. 11. The rotational coherence ρ_{ab} exhibits an asymmetry with respect to the vibrational detuning, which is the result of the rotational Stark shift (proportional to the field intensities of the 1084 and 1064 nm sideband). We believe that the small modulation feature in the vibrational coherence ρ_{ac} around 0.5 GHz is due to the different pulse durations of the driving fields. In the case that all pulses have identical temporal profiles, we observe a strong modulation of the coherences, possibly due to the Rabi flopping. This feature becomes more washed out if pulse lengths are not matched.

Similar to the approach in Ref. [4], we derive a new propagation equation for rotational-vibrational sideband $E_{q,p}$, which includes cross-coupling terms due to the coherence ρ_{bc}:

$$
\begin{aligned}
\frac{\partial E_{q,p}(z)}{\partial z} = &\, i\eta\hbar N\omega_{q,p}(a_{q,p}\rho_{aa}E_{q,p} + d^1_{q,p}\rho_{bb}E_{q,p} + d^2_{q,p}\rho_{cc}E_{q,p} \\
&+ \rho_{ab}b^1_{q+1,p}E_{q+1,p} + \rho^*_{ab}b^1_{q,p}E_{q-1,p} + \rho_{ac}b^2_{q,p+1}E_{q,p+1} \\
&+ \rho^*_{ac}b^2_{q,p}E_{q,p-1} + \rho_{bc}b^3_{q-1,p+1}E_{q-1,p+1} \\
&+ \rho^*_{bc}b^3_{q,p}E_{q+1,p-1}).
\end{aligned}
\tag{3}
$$

Here the coefficient η represents the impedance of free space $\eta=\mu/\epsilon_0$, with N representing the number of molecules per unit volume.

The constants $a_{q,p}$, $b^1_{q,p}$, $b^2_{q,p}$, $b^3_{q,p}$, $d^1_{q,p}$, and $d^2_{q,p}$ include all contributions from allowed vibrational and rotational transitions in Lymann and Werner bands. We retain 13 rotational
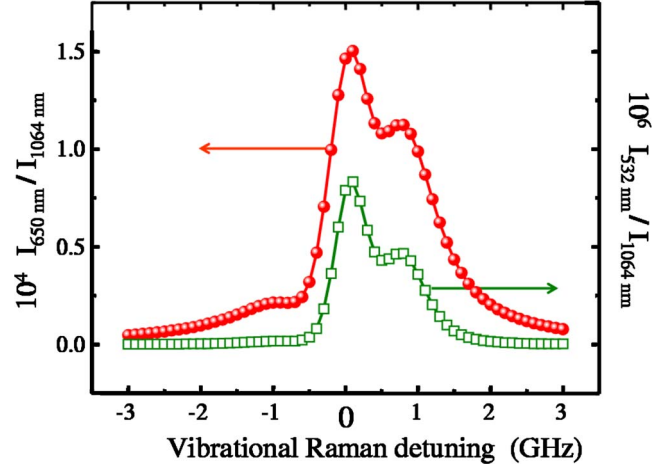

FIG. 12. (Color online) Calculated intensities of the vibrational anti-Stokes sidebands 650 and 532 nm produced by the two input lasers (1064 and 807 nm) as a function of their detuning from the vibrational Raman resonance and after a propagation distance of 1.1 mm in a cell filled with D_2. The results are normalized to the input peak intensity of the Nd:YAG laser.

sidebands and 10 vibrational sidebands, apply the driving fields $E_{-1,0}$ at a wavelength of 1084 nm, $E_{0,0}$ at 1064 nm, and $E_{0,1}$ at 807 nm at the input of the cell filled with D_2 (density $N=2.69\times10^{19}$ molecules/cm^3), and solve the coupled system of equations for a small propagation distance of 1.1 mm. This small propagation distance insures that the evolution of the system remains consistent under the initial conditions for populations and coherences in Fig. 11. As more sidebands are generated in the cell, the propagation equations need to be solved self-consistently, with coherences and populations recalculated at each step. These results will require much more extensive detailed calculations which are beyond the scope of this paper.

After propagation in the cell, the intensities of generated sidebands are calculated as a function of the vibrational Raman detuning and as a function of time. We present in Figs. 12 and 13 the calculated intensities of some of the rotational and vibrational sidebands at a time corresponding to the peak pulse intensity as the detuning is changed across vibrational Raman resonance. The behavior of rotational and vibrational sidebands is remarkably close to the experimental curves. The enhancement of rotational sidebands at positive values of Raman detunings is not only due to the rotational Stark shifts, but also due to the rovibrational coherence ρ_{bc}, which gives a constructive interference between the intensities of the generated rotational and vibrational combs and the rovibrational comb of frequencies. We expect that when the sidebands propagate further, the enhancement of rotational sidebands becomes more dramatic.

In summary, we demonstrate that two independent processes (SRS and molecular modulation) can be coupled for efficient generation of more than two octaves of coherent bandwidth, possibly leading to improved laser field shaping. In addition, the increase of the density of the generated comb could be used for high intensity ultrafast laser field applications.
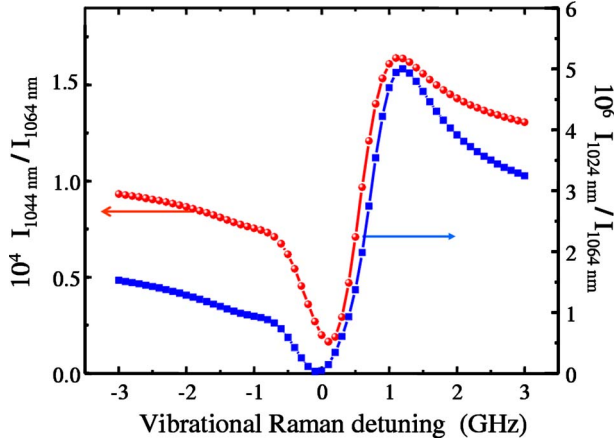
FIG. 13. (Color online) Calculated intensities of the rotational anti-Stokes sidebands 1044 and 1024 nm produced by the two input lasers (1064 and 1084 nm) as a function of their detuning from the vibrational Raman resonance after a propagation distance of 1.1 mm in a cell filled with D_2. The results are normalized to the input peak intensity of the Nd:YAG laser.

ACKNOWLEDGMENTS

APPENDIX

The dispersion and coupling coefficients read:

$$a_{q,p} = \frac{1}{2\hbar^2} \sum_i \left[\frac{|\mu_{ai}|^2}{(\omega_i - \omega_a) - \omega_{q,p}} + \frac{|\mu_{ai}|^2}{(\omega_i - \omega_a) + \omega_{q,p}} \right],$$

(A1)

$$b_{q,p}^1 = \frac{1}{2\hbar^2} \sum_i \left[\frac{\mu_{ai}\mu_{bi}^*}{(\omega_i - \omega_a) - \omega_{q,p}} + \frac{\mu_{ai}\mu_{bi}^*}{(\omega_i - \omega_b) + \omega_{q,p}} \right],$$

(A2)

$$b_{q,p}^2 = \frac{1}{2\hbar^2} \sum_i \left[\frac{\mu_{ai}\mu_{ci}^*}{(\omega_i - \omega_a) - \omega_{q,p}} + \frac{\mu_{ai}\mu_{ci}^*}{(\omega_i - \omega_c) + \omega_{q,p}} \right],$$

(A3)

$$b_{q,p}^3 = \frac{1}{2\hbar^2} \sum_i \left[\frac{\mu_{bi}\mu_{ci}^*}{(\omega_i - \omega_b) - \omega_{q,p}} + \frac{\mu_{bi}\mu_{ci}^*}{(\omega_i - \omega_c) + \omega_{q,p}} \right],$$

(A4)

$$d_{q,p}^1 = \frac{1}{2\hbar^2} \sum_i \left[\frac{|\mu_{bi}|^2}{(\omega_i - \omega_b) - \omega_{q,p}} + \frac{|\mu_{bi}|^2}{(\omega_i - \omega_b) + \omega_{q,p}} \right],$$

(A5)

$$d_{q,p}^2 = \frac{1}{2\hbar^2} \sum_i \left[\frac{|\mu_{ci}|^2}{(\omega_i - \omega_c) - \omega_{q,p}} + \frac{|\mu_{ci}|^2}{(\omega_i - \omega_c) + \omega_{q,p}} \right],$$

(A6)

where $\mu_{\alpha\beta}$ are the dipole moments of the transition $\alpha \rightarrow \beta$.

[1] M. Drescher, M. Hentschel, R. Kienberger, G. Tempea, Ch. Spielmann, G. A. Reider, P. B. Corkum, and F. Krausz, Science **291**, 1923 (2001).

[2] P. M. Paul, E. S. Toma, P. Breger, G. Mullot, F. Augi, P. Balcou, H. G. Muller, and P. Agostini, Science **292**, 1689 (2001).

[3] F. Krausz, Phys. World **14**, 41 (2001).

[4] S. E. Harris and A. V. Sokolov, Phys. Rev. A **55**, R4019 (1997); S. E. Harris and A. V. Sokolov, Phys. Rev. Lett. **81**, 2894 (1998).

[5] A. V. Sokolov and S. E. Harris, J. Opt. B: Quantum Semiclassical Opt. **5**, R1 (2003).

[6] A. V. Sokolov, D. R. Walker, D. D. Yavuz, G. Y. Yin, and S. E. Harris, Phys. Rev. Lett. **85**, 562 (2000).

[7] A. V. Sokolov, D. R. Walker, D. D. Yavuz, G. Y. Yin, and S. E. Harris, Phys. Rev. Lett. **87**, 033402 (2001).

[8] M. Y. Shverdin, D. R. Walker, D. D. Yavuz, G. Y. Yin, and S. E. Harris, Phys. Rev. Lett. **94**, 033904 (2005).

[9] E. M. Belenov, A. V. Nazarkin, and I. P. Prokopovich, Pis'ma Zh. Eksp. Teor. Fiz. **55**, 223 (1992).

[10] E. M. Belenov, P. G. Kryukov, A. V. Nazarkin, and I. P. Prokopovich, Zh. Eksp. Teor. Fiz. **105**, 28 (1994).

[11] A. Nazarkin, G. Korn, M. Wittmann, and T. Elsaesser, Phys. Rev. Lett. **83**, 2560 (1999).

[12] D. D. Yavuz, D. R. Walker, and M. Y. Shverdin, Phys. Rev. A **67**, 041803(R) (2003).

[13] A. E. Kaplan, Phys. Rev. Lett. **73**, 1243 (1994).

[14] S. E. Harris, D. R. Walker, and D. D. Yavuz, Phys. Rev. A **65**, 021801(R) (2002).

[15] D. D. Yavuz, D. R. Walker, M. Y. Shverdin, G. Y. Yin, and S. E. Harris, Phys. Rev. Lett. **91**, 233602 (2005).

[16] M. Katsugarawa, Y. Ono, F. le Kien, and K. Hakuta, CLEO/IQEC 2004, Technical Digest CMO6 (2004).

[17] C. S. Wang, Phys. Rev. **182**, 482 (1969).

[18] G. Eckhardt, R. W. Hellwarth, F. J. McClung, S. E. Schwartz, D. Weiner, and E. J. Woodbury, Phys. Rev. Lett. **9**, 455 (1962).

[19] M. Geller, D. P. Bortfeld, and W. R. Sooy, Appl. Phys. Lett. **3**, 36 (1963).

[20] G. Eckhardt, D. P. Bortfeld, and M. Geller, Appl. Phys. Lett. **3**, 137 (1963).

[21] R. W. Minck, R. W. Terhune, and W. G. Rado, Appl. Phys. Lett. **3**, 181 (1963).

[22] H. Otsuka and T. Imasaka, Opt. Commun. **237**, 417 (2004).

[23] T. Imasaka, S. Kawasaki, and N. Ishibashi, Appl. Phys. B: Photophys. Laser Chem. **B49**, 389 (1989).

[24] T. Imasaka, T. Higashijima, S. Kawasaki, and N. Ishibashi, Appl. Phys. B: Photophys. Laser Chem. **B56**, 259 (1993).

[25] S. Yoshikawa and T. Imasaka, Opt. Commun. **96**, 94 (1993).

[26] S. Yoshikawa, S. Kawasaki, T. Imasaka, and N. Ishibashi, Jpn. J. Appl. Phys., Part 2 **30**, L283 (1991).

[27] B. N. Perry, P. Rabinowitz, and D. S. Bomse, Opt. Lett. **10**, 146 (1985).

[28] M. R. Perrone, V. Picino, G. D. Nunzio, and V. Nassisi, IEEE J. Quantum Electron. **33**, 938 (1997).

[29] A. M. Burzo, A. V. Chugreev, and A. V. Sokolov, Opt. Commun. **264**, 454 (2006).

[30] K. D. V. den Hout, P. W. Hermans, E. Mazur, and H. F. P. Knaap, Physica A **104**, 509 (1980).

[31] C. G. Morgan, Rep. Prog. Phys. **38**, 621 (1975).

[32] A. H. Guenther and J. R. Bettis, IEEE J. Quantum Electron. **QE 3**, 581 (1967).

[33] S. Gundry, M. P. Anscombe, A. M. Abdulla, S. D. Hogan, E. Sali, J. W. G. Tish, and J. P. Marangos, Phys. Rev. A **72**, 033824 (2005).

[34] F. Le Kien, J. Q. Liang, M. Katsuragawa, K. Ohtsuki, K. Hakuta, and A. V. Sokolov, Phys. Rev. A **60**, 1562 (1999).

[35] D. R. Walker, D. D. Yavuz, M. Y. Shverdin, G. Y. Yin, A. V. Sokolov, and S. E. Harris, Opt. Lett. **27**, 2094 (2002).